Molecular dynamics simulation of fluoride-perovskites

1992 J. Phys.: Condens. Matter 4 2097

(http://iopscience.iop.org/0953-8984/4/8/023)

J. Phys.: Condens. Matter 4 (1992) 2097–2108. Printed in the UK

Molecular dynamics simulation of fluoride–perovskites

G W Watson, S C Parker and A Wall
School of Chemistry, University of Bath, Claverton Down, Bath BA2 7AY, UK

Received 23 August 1991, in final form 6 November 1991

Abstract. We present the results from constant-pressure constant-temperature molecular dynamics simulations on the fluoride–perovskites: $KMnF_3$, $KZnF_3$ and $KCaF_3$. These simulations lead to the predictions that $KMnF_3$ and $KZnF_3$ are not superionic conductors while $KCaF_3$ shows limited superionic behaviour with a diffusion coefficient of 5.24×10^{-6} cm^2 s^{-1} ($\sigma = 0.145\ \Omega^{-1}$ cm^{-1}) and $T_c = 0.93\ T_m$. However, these results are only qualitative since the use of the rigid-ion model resulted in simulated temperatures above the experimental melting points.

1. Introduction

The electrical conductivity of fluoride–perovskites has been studied using a number of experimental and theoretical methods, including NMR [1], neutron scattering [2], ionic conductivity studies [1, 3–5] and molecular dynamics (MD) simulation [6]. Some of these studies have focused on fluoride–perovskites as structural analogues for the mantle-forming mineral (Mg, Fe)SiO_3–perovskite [2, 4, 6]. (Mg, Fe)SiO_3–perovskite is thought to be the dominant phase in the Earth's lower mantle [7] and hence accounts for approximately 40% of the Earth by volume. However, studies of this material under lower mantle conditions (P = 20–135 GPa; T = 2000–3000 K) are very difficult, and alternative approaches such as simulation and analogue studies have been used. Earlier MD studies of $MgSiO_3$–perovskite show that it may be a superionic conductor (i.e. it exhibits ionic conductivity comparable in magnitude with that observed in the molten salt) at high temperatures and pressures [8, 9]. Such high-temperature and high-pressure behaviour would have important implications for geological theories of the creep of the mantle and the generation of the Earth's magnetic field [5, 10]. However, recent ionic conductivity experiments by Li and Jeanloz [11–13] were unable to detect any type of conductivity in $MgSiO_3$–perovskite. The study by Peyronneau and Poirier [10] of conductivity in this material led to a different conclusion. Extrapolation of their electronic conductivity measurements to mantle conditions predicted conductivity. Additionally they could not rule out a possible contribution from superionic conductivity and hence there is still much controversy surrounding this silicate–perovskite.

Superionic conductivity has been associated with a phase change [14] or 'melting' of a sublattice [15]. In the case of fluoride–perovskites, this is thought to be due to the onset of a high fluoride mobility a few hundred Kelvin below their melting points. This phenomenon is normally ascribed to the melting of the fluoride sublattice but is more accurately described as a concerted hopping motion. The most widely studied superionic

0953-8984/92/082097 + 12 $04.50

conductor in which the fluoride sublattice has a high mobility is CaF_2. It has been extensively modelled by MD [6, 16–18] and consequently it can be used as a bench mark for MD codes. Thus we have simulated CaF_2 to confirm the reliability of our approach.

The aim of this work is to use MD and lattice dynamics to look for superionic conductivity in the fluoride–perovskites: $KMnF_3$, $KCaF_3$ and $KZnF_3$. $KMnF_3$ was chosen because we believe it not to be a superionic conductor, whereas NMR relaxation studies and ionic conductivity measurements have shown that superionic conductivity occurs in $KCaF_3$ several hundred Kelvin below its melting point [1]. Finally, $KZnF_3$ was chosen because of the controversy which surrounds this material. Measurements of the conductivity and viscosity led Poirier *et al* [5] to claim that $KZnF_3$ is a superionic conductor. The onset of superionic conductivity was associated with a marked decrease in the viscosity. This result, however, was contradicted by the ionic conductivity measurements of Anderson *et al* [3], and by the neutron scattering work of Ridou *et al* [2].

The theoretical methods used to investigate the perovskites are described in the next section.

2. Theoretical methods

The two methods used in this work for modelling solids at finite temperatures and pressures are lattice dynamics and MD. Our lattice dynamics approach uses the quasi-harmonic approximation, in which the lattice vibrations are considered to be a series of quantized harmonic oscillators, the frequency of which vary with the unit-cell volume [26]. This approximation is strictly only valid at temperatures well below the melting point when anharmonic effects are not important. MD treats the anharmonic effects explicitly and is therefore valid up to and beyond the melting point. MD is the main technique used in this paper and is described in more detail in the next section.

3. Molecular dynamics technique

The MD technique was developed in the 1950s to study liquids [19], but it has been extensively used to study ionic crystals, and especially their superionic conductivity [6, 16–18].

The method consists of treating a box of N ions and solving Newton's laws of motion over a finite time period via an iterative process. Initially the ions are assigned random velocities such that

$$\sum_i m_i v_i(0) = 0 \qquad \sum_i m_i [v_i(0)]^2 = 3Nk_B T$$

where N is the number of ions in the simulation box, k_B is the Boltzmann constant and T is the simulation temperature.

The forces acting on the ions are described by the interatomic potentials, in this case a full charge interaction with a short-range Buckingham potential of the form

$$F_i = \sum_j^{\text{crystal}} \left[-\frac{q_i q_j}{r_{ij}^2} - \frac{A_{ij}}{\rho_{ij}} \exp\left(-\frac{r_{ij}}{\rho_{ij}}\right) + \frac{6C_{ij}}{r_{ij}^7} \right]$$

where q_i and q_j are the charges of ions i and j separated by a distance r_{ij} and A, ρ and C

are potential parameters. Thus the forces on any one ion can be calculated and the new velocity and position calculated for an infinitely small time step by solving Newton's laws of motion:

$$F_i(t) = m_i a_i(t)$$

$$r_i(t + \mathrm{d}t) = r_i(t) + v_i(t)\,\mathrm{d}t$$

$$v_i(f + \mathrm{d}t) = v_i(t) + a_i(t)\,\mathrm{d}t.$$

However, using finite time steps, these expressions are inadequate; in this study a fifth-order predictor corrector method due to Gear [20] was used.

The choice of $\mathrm{d}t$ in these simulations is also important. If $\mathrm{d}t$ is too large, lattice vibrations can occur within the time step, leading to gross errors. If $\mathrm{d}t$ is too small, the simulations will exceed the computer time available. In this set of calculations a time step of 10^{-15} s was used, allowing simulations of about 10^{-11} s (10 ps).

A further constraint imposed by the availability of computer time was that only the trajectories of about 1000 particles are considered explicitly. A periodic boundary condition is applied to eliminate the effect of the surface. The box is surrounded by images of itself such that, if a particle leaves the box, it re-enters on the opposite face with the same trajectory. This imposes an artificial repetition of the crystal lattice and removes the possibility of forming Schottky defects spontaneously. Such defects must therefore be set up in the initial box by the removal of ions. We felt that it was important to perform simulations on cell containing these defects to investigate their effect on the superionic conductivity and melting points. Frenkel defects can still form spontaneously.

The first stage of MD simulations is to allow the system to come to equilibrium at the simulation temperature before any data are collected. This was achieved by scaling runs of between 4000 and 5000 time steps (4–5 ps) in which the velocities of the ions were periodically scaled to the simulation temperature. Additional scaling was performed on those systems in which large temperature fluctuations, greater than 50 K, were still found, and on those systems close to the simulated melting point. Data were then collected during runs of between 2000 and 5000 time steps (2–5 ps). Additional longer simulations were performed on those systems in which superionic conductivity was predicted, and on those systems which were close to the simulated melting point.

During all these simulations the constant-pressure constant-temperature MD technique was used. Constant-pressure MD [21] allows a dynamic change in both the lattice vectors and the angles with time. Constant-temperature MD [22, 23] places the simulation box in contact with a heat bath, this contact being distributed throughout the system. Energy is free to transfer into or out of the simulation box and this has the effect of keeping the system at constant temperature but still allows for localized changes where potential energy is transferred to kinetic energy. This method thus uses an isobaric–isothermal ensemble (P, T, N).

The data from MD that we have used to study atomic transport are the mean square displacements (MSD) and the radial distribution functions (RDF). The MSD represents the average displacement of an ion type from its initial coordinates, given by

$$\langle r_i^2 \rangle = \frac{1}{N_i} \sum_i \{[x_i(t) - x_i(0)]^2 + [y_i(t) - y_i(0)]^2 + [z_i(t) - z_i(0)]^2\}.$$

This is calculated periodically and, if no increase in MSD is observed with time, the atoms are merely vibrating about their mean lattice sites. If the MSD of one ion type

increases with time, then diffusion of that ion type is indicated. The diffusion coefficient D_i is the gradient of the graph of the MSD with time:

$$\langle r_i^2 \rangle = 6D_i t + B_i$$

where B_i is the Debye–Waller factor. From the diffusion coefficient it is possible to use the Nernst–Einstein equation to estimate the conductivity

$$\sigma = Nq^2 D_i / f k_B T$$

where N is the density of charge carriers per unit volume, q is the charge on the charge carrier, D_i is the tracer diffusion coefficient, f is a correlation factor, k_B is the Boltzmann constant and T is the temperature. The correlation factor f depends on the diffusion mechanism and the lattice structure and allows for the fact that successive jumps of the tracer may be concerted whereas those of the defect are random. This is usually between 0.5 and 0.8 but has been set to unity for this purpose since we wish only to establish the order of magnitude of the diffusion.

The RDF provides a measure of the long-range order in the crystal lattice. This gives the ensemble average for the number of ions of type A at a given distance from a central ion of type B.

The simulated melting points were determined by the use of the MSDs. We consider the crystal to have melted when all sublattices show an increase in MSD with time. Such temperatures were determined by heating the simulation in steps of 50 K until this occurred. At this point an additional simulation was performed to heat the system rapidly to melting, to confirm that the temperature was independent of the rate of heating, within the limitations of computer CPU time.

4. Potentials

The short-range potential parameters for CaF_2 [24], $KZnF_3$ and $KMnF_3$ [25] were chosen because of their proven ability to reproduce both the pure and the defect lattice properties and energies. Additionally, the potentials for $KZnF_3$ and $KMnF_3$ model the phonon dispersion curves well [25]. The potential for $KCaF_3$ was obtained by combining the potentials developed for CaF_2 and the potassium–fluorine interaction from $KMnF_3$ and $KZnF_3$.

The interatomic potential for the fluorine–fluorine interaction, common to all the systems, was a spline potential. Complementary lattice dynamics studies show discontinuities in some of the crystal properties with increasing volume. Thus, we fitted the spline potential to a Buckingham form by using a least-squares fitting procedure. The fitted potential gives excellent agreement with the spline potential for fluorine–fluorine distances above 2.3 Å.

The potassium–fluorine interaction, common to all three fluoride–perovskites, was also fitted to remove the $-D/r^8$ term.

An important limitation of the MD technique is that only rigid-ion models can be considered, i.e. no account was taken of the electronic polarizability. The full valence charges were thus placed on the ions and were summed using the Ewald method. The potential parameters thus derived are shown in table 1.

The potential parameters for $KMnF_3$ and $KZnF_3$ once the shell model is removed look similar. Therefore, a series of free-energy minimizations was carried out, with and without the shell model, using the computer code PARAPOCS [26]. The results of the

Table 1. Interatomic potential parameters.

Interaction	A (eV)	ρ (A)	C (eV A^6)
F–F	99 731 833.990	0.120 13	17.024 23
Ca–F	1 272.800	0.299 70	0.00
K–F	2 674.306	0.283 52	30.273 93
Zn–F	1 655.530	0.265 16	0.00
Mn–F	1 654.780	0.275 91	0.00

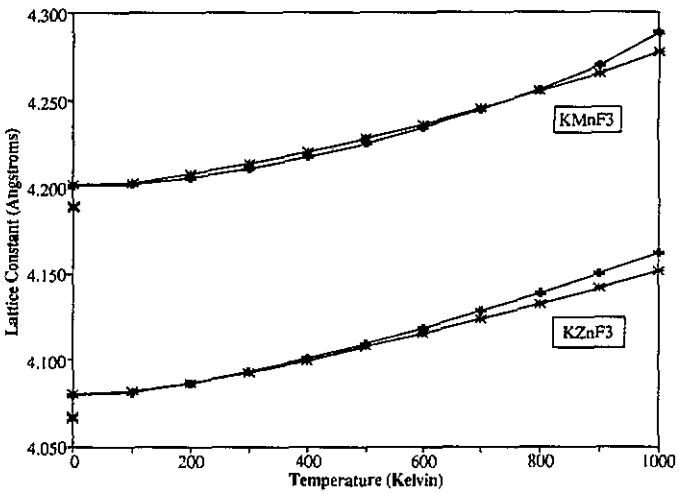

Figure 1. Variation in lattice constant with temperature for $KMnF_3$ and $KZnF_3$: *, shell model; +, rigid-ion model; × excluding zero-point energy

change in lattice constant with temperature are shown in figure 1. These indicate that the rigid-ion potentials faithfully reproduce the structure of these systems, which gives us confidence in using both potentials to investigate the structural behaviour with temperature. In addition the figure shows the effect of including explicitly the zero-point energy. This leads to lattice expansion, which is not treated in most static minimization or MD. The lattice constant neglecting the zero-point energy is also shown.

5. Molecular dynamics simulation of CaF_2

CaF_2, a well established superionic conductor, has been extensively modelled by MD [6, 16–18] and thus simulation of this system was considered to be a suitable test of confirm the reliability of our approach and potentials. CaF_2 was simulated in an MD box of 768 ions with four unit cells in the X, Y and Z directions. Pure systems, i.e. systems without defects, were investigated first.

At 300 K, no superionic conductivity is predicted, indicated by a constant MSD with time (figure 2). The RDFs (not included) show well defined peaks, indicating that the extensive long-range order of the crystal is preserved.

At 1600 K, an increase in MSD of the fluoride ions with time is observed, while the calcium ions remain on their lattice sites, indicating superionic conductivity (figure 3). The RDFs show the loss of long-range order of the fluoride sublattice while the calcium sublattice retains its long-range order.

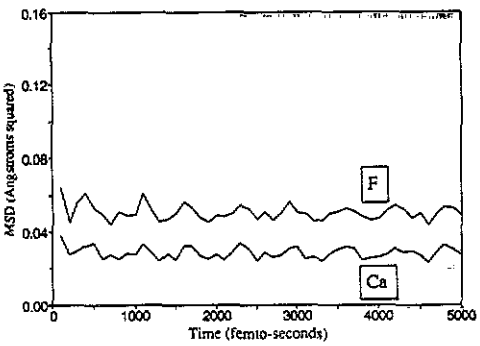

Figure 2. MSD plot for CaF_2 at 300 K.

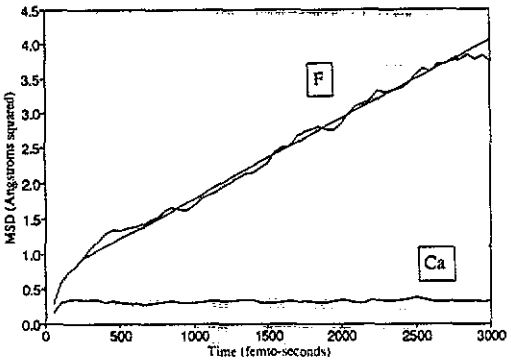

Figure 3. MSD plot for CaF_2 at 1600 K.

Schottky defects were created by removing one Ca and two F ions from the MD supercell to introduce vacancies. These vacancies were placed as far apart as possible. Simulations of the defective CaF_2 produced results almost identical with those of the pure systems. The melting points for CaF_2 were also identical, 2200 K, in comparison with the experimental value of 1696 K [3]. The problem of elevated melting points is discussed later.

The diffusion constant calculated from the MSD ($1.9 \times 10^{-5}\,cm^2\,s^{-1}$) shows good agreement with the values obtained by Rahman [17] ($2.6 \times 10^{-5}\,cm^2\,s^{-1}$) and by Cheeseman and Angel [6] ($2.5 \times 10^{-5}\,cm^2\,s^{-1}$). Using the Nernst–Einstein equation our diffusion coefficient corresponds to a conductivity of $0.944\,\Omega^{-1}\,cm^{-1}$. This is in good agreement with the ionic conductivity measurements of O'Keeffe [27] ($\sigma = 1.0\,\Omega^{-1}\,cm^{-1}$) and the calculated value of Cheeseman and Angel [6] ($\sigma = 1.2\,\Omega^{-1}\,cm^{-1}$). The modelling of CaF_2 has thus shown that the MD technique employed in this study is suitable for investigation of superionic behaviour.

The next section describes the simulations performed on the fluoride–perovskites $KMnF_3$, $KZnF_3$ and $KCaF_3$.

6. Molecular dynamics simulation of $KMnF_3$, $KZnF_3$ and $KCaF_3$

The starting ionic coordinates for the MD were obtained from free-energy minimizations at 300 K using the computer codes PARAPOCS [26]. This predicted a cubic structure for $KMnF_3$ and $KZnF_3$, and an orthorhombic structure for $KCaF_3$, consistent with

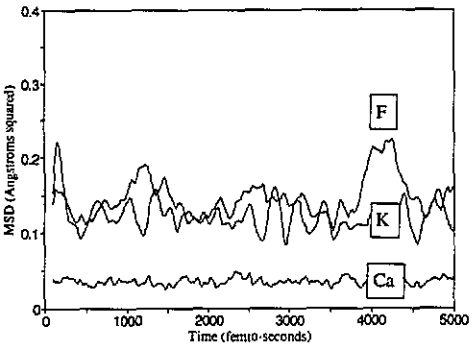

Figure 4. MSD plot for $KCaF_3$ at 300 K.

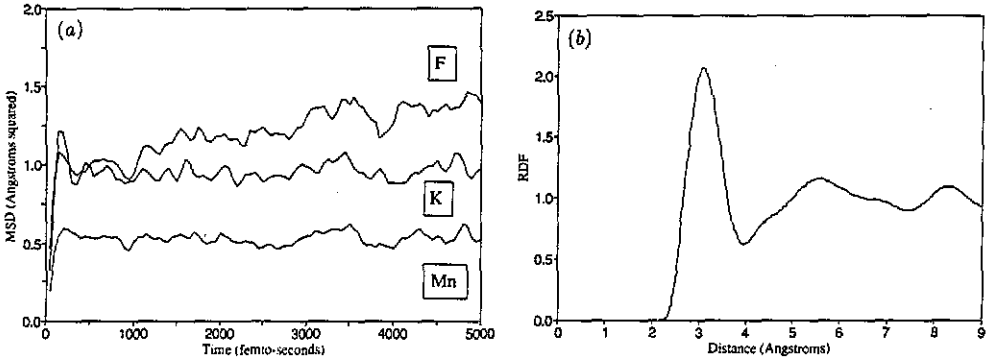

Figure 5. (*a*) MSD plot for $KMnF_3$ at 2275 K. (*b*) Fluorine–fluorine RDF of $KMnF_3$ at 2275 K.

experimental observations [25, 28]. The MD simulations were then carried out on an MD box of 1280 ions with four orthorhombic unit cells in each of the X, Y and Z directions.

Once again both pure and defect simulations were performed. The defects in the latter case were K and F ion vacancy pairs (pseudo-Schottky), because they represent the lowest-energy defect [25]. The results were found to be almost independent of the introduction of the defects.

The MSDs of all three systems (with defects) at 300 K show no increase with time ($KCaF_3$ is shown in figure 4). The RDFs of all the systems are very similar except for the F–F RDF of $KCaF_3$ which shows more structure because of its orthorhombic space group. All show that the extensive long-range order is preserved. These results indicate that no diffusion occurs in any system at 300 K.

On simulation at elevated temperatures, $KMnF_3$ and $KZnF_3$ show no increase in the MSD of fluoride ions with time to within 50 K of the MD melting temperature. These conclusions are demonstrated by figure 5(*a*) ($KMnF_3$ at 2275 K) and figure 6(*a*) ($KZnF_3$ at 2200 K). The accompanying F–F RDFs (figures 5(*b*) and 6(*b*)) show the onset of the loss of long-range order associated with the approach of the melting point.

$KCaF_3$, however, shows an increase in MSD with time 150 K from its MD melting point (2100 K). The MSD at 1950 K, shown in figure 7(*a*), results in a diffusion coefficient of $5.24 \times 10^{-6}\,cm^2\,s^{-1}$ and a conductivity σ of $0.145\,\Omega^{-1}\,cm^{-1}$. The diffusion coefficient increases rapidly with increasing temperature and at 2100 K (figure 8) has a value of $1.48 \times 10^{-5}\,s^{-1}$ ($\sigma = 0.393\,\Omega^{-1}\,cm^{-1}$).

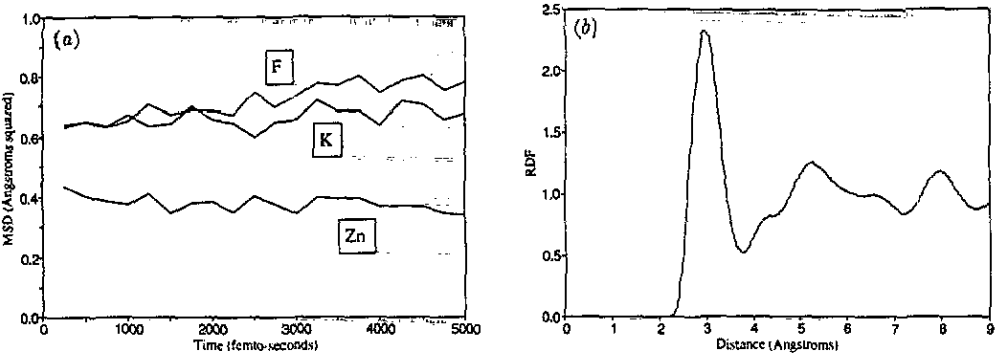

Figure 6. (*a*) MSD plot for $KZnF_3$ at 2200 K. (*b*) Fluorine–fluorine RDF of $KZnF_3$ at 2200 K.

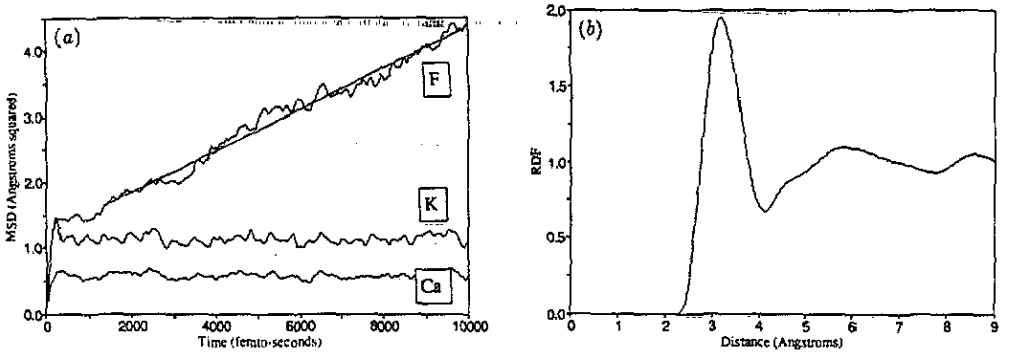

Figure 7. (*a*) MSD plot for $KCaF_3$ at 1950 K. (*b*) Fluorine–fluorine RDF of $KCaF_3$ at 1950 K.

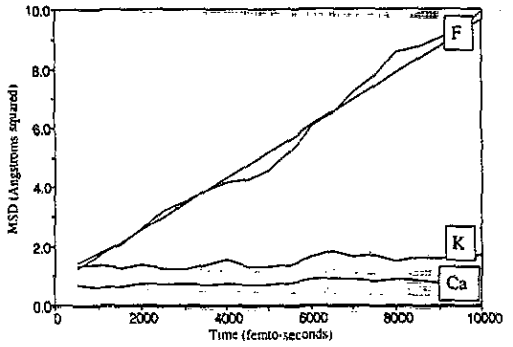

Figure 8. MSD plot for $KCaF_3$ at 2000 K.

The F–F RDF 2050 K (figure 7(*b*)) indicates the breakdown of the fluorine sublattice, while the potassium and calcium sublattices show long-range order. However, the RDF is misleading since the F–F RDF for both $KMnF_3$ and $KZnF_3$ also show a breakdown in

Table 2. Comparison of pure and defect simulation melting points with experimental values.

System	Melting point of the system (K)		
	Pure	Defect	Experimental
$KMnF_3$	2450	2350	?
$KZnF_3$	2600	2250	1143(5)
$KCaF_3$	2100	2075	?

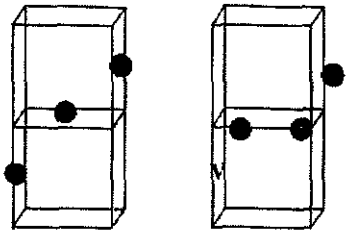

Figure 9. Formation of a vacancy V and an interstitial pair.

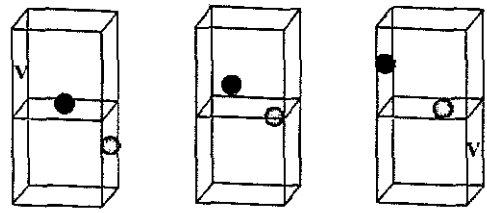

Figure 10. Concerted hopping motion of two fluoride ions showing the migration of a vacancy V in 0.35 ps.

the fluorine sublattice, although no superionic conductivity is predicted. The RDF is, therefore, not considered a good predictor of superionic conductivity.

One area in which the defect and pure simulations did not agree was in the melting point. Table 2 shows the MD melting points for the three systems for both pure and defect structures in comparison with the experimental values where available.

7. Mechanism of fluoride ion diffusion in $KCaF_3$

A trajectory analysis of the $KCaF_3$ system at 1950 K was performed using Insight II [29]. Coordinates and velocities were collected and stored every 25 fs for later analysis.

The motions of the fluoride ions were animated to study their diffusion mechanism. The formation of vacancies was observed to occur by the production of fluoride pairs occupying interstitials around a lattice site (figure 9). Vacancies were observed to have lifetimes as long as 0.75 ps.

These vacancies move through the system by hopping of the fluoride ions, often in correlated motion, involving between one and five ions. An example of a two-ion correlated hop is shown in figure 10, which took 0.35 ps to occur.

The mechanism thus postulated is that of a vacancy mechanism with partially correlated hopping of the fluoride ions across the edges of the fluoride octahedra.

8. Discussion

Our MD simulations predict only the rapid diffusion of fluoride ions in $KCaF_3$. No indication of superionic behaviour is apparent in the other perovskites up to 50 K below

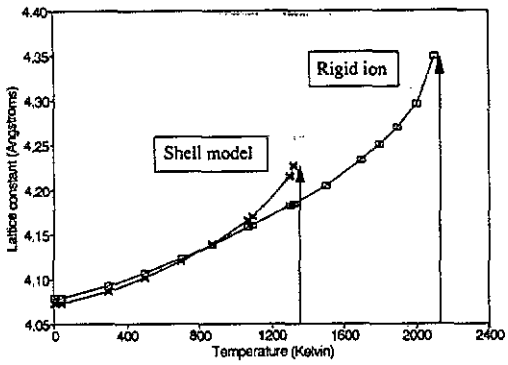

Figure 11. Temperature of the breakdown of the quasi-harmonic approximation using rigid-ion and shell models.

their simulated melting points. This indicates a good degree of sensitivity of the technique since these results were obtained using a common set of potentials. However, the melting points obtained are in excess of the experimental values.

Previous MD studies have also predicted melting points in excess of the experimental observations [14]. This problem may arise because of a number of shortcomings of the technique. Firstly, at present MD only considers rigid-ion models because of the limits of computer time. However, the dielectric constant of a material is very sensitive to polarizability and the removal of the shell model results in a lower dielectric constant. For very simple systems, it is possible to refit the potentials to reproduce the dielectric constant; for more complex systems this becomes difficult and has not been done for the fluoride–perovskites. A lower dielectric constant results in an overestimate of the defect energies compared with those produced by the shell model [30]. This will result in a reduction in the relative stability of the melt because of its defect structure, leading to a higher melting point. This argument can also be extended to the onset of superionic conductivity. The movement of fluoride ions generally occurs by a hopping mechanism; the activation energy is dependent on the dielectric constant. Thus both the melting temperature and the temperature at which superionic conductivity occurs should be raised to a similar degree by the use of a rigid-ion potential.

This argument is supported by simulations performed using the lattice dynamics code PARAPOCS [26]. Simulation of $KZnF_3$ was undertaken using the same potentials as used in the MD, but with and without the shell model. The result of the change in lattice constant with temperature is shown in figure 11. The use of the shell model leads to a lattice instability (breakdown of quasi-harmonic approximation, preceding melting) at a lower temperature than the rigid-ion model and hence results in the prediction of elevated melting points with the use of a rigid-ion model.

Secondly, the use of a periodic boundary condition eliminates all surfaces. Solids are known to melt from the surfaces and their absence from the simulation will modify this process. Intuitively it can be said that, if melting initially occurs at a surface, the absence of such a surface would lead to a higher activation energy of melting and a higher predicted melting point.

It is thus our belief that, although the onset on superionic conductivity in $KCaF_3$ was above the experimental melting point, the result is qualitatively valid, since both melting

and superionic conductivity are affected to a similar degree by the use of a rigid ion potential.

The scale of the superionic behaviour ($\sigma = 0.145\ \Omega^{-1}\ cm^{-1}$) is less than that of CaF_2 ($\sigma = 0.944\ \Omega^{-1}\ cm^{-1}$) and occurs across a much smaller temperature range, $T_c = 0.93T_m$ and $T_c = 0.73T_m$ for $KCaF_3$ and CaF_2, respectively. It would therefore be harder to detect superionic conductivity in $KCaF_3$ experimentally.

The defective and pure systems produced melting points at different temperatures. It is thought that the removal of an ion will result in lower defect energies around the vacancy. This will encourage the production of defects, leading to a lower melting point. The reason why the superionic conductors did not show a reduction in melting point was that such defects were already forming below the melting point and thus the introduction of defects had little effect.

9. Conclusions

Our simulations predict that $KCaF_3$ is a superionic conductor, in agreement with the NMR studies of Chadwick *et al* (1). The mechanism postulated from trajectory analysis is that of a locally correlated vacancy mechanism.

We have also concluded that $KZnF_3$ is not a superionic conductor, in contradiction to the results of Poirier *et al* [5] but in agreement with those of Anderson *et al* [3] and Ridou *et al* [2]. Our results also show $KMnF_3$ not to be a superionic conductor.

Additionally we have shown by the use of both MD and lattice dynamics that the shell model is vital to obtaining properties such as superionic conductivity and melting points at temperatures close to the experimental values. The lattice dynamics simulations indicated the extent of the change in melting and superionic conductivity temperature when converting from a shell model to a rigid-ion model. We thus feel that it is imperative to develop MD codes which incorporate the shell model, even though this will cause the codes to be even more computationally expensive.

Acknowledgments

We would like to thank M Matsui for his help in starting this project, G D Price and J P Poirier for suggesting this line of research and M Gillan and A Chadwick for reviewing the manuscript. We would also like to thank the National Environment Research Council for research grant GR3/6970, and the receipt of a research studentship, and the Science and Engineering Research Council for research grant GR/G 13990. Finally we thank Biosym Tech. Inc. for access to their graphics software.

References

[1] Chadwick A V, Strange J H, Ranieri G A and Terenzi M 1983 *Solid State Ion.* **9** 555–8
[2] Ridou C, Rousseau M, Pernot B and Bouillot J 1986 *J. Phys. C: Solid State Phys.* **19** 4847–53
[3] Anderson N H, Kjems J K and Hayes W 1985 *Solid State Ion.* **17** 143–5
[4] O'Keeffe M and Bovin J O 1979 *Science* **206** 599–600
[5] Poirier J P, Peyronneau J, Gesland J Y and Brebec G 1983 *Phys. Earth Planetary Interiors* **32** 273–87
[6] Cheeseman P A and Angel C A 1981 *Solid State Ion.* **5** 597–600
[7] Knittle E and Jeanloz R 1987 *Science* **235** 668–70

[8] Wall A and Price G D 1989 *Phys. Earth and Planetary Interiors* **58** 192–204
[9] Kapusta B and Guillope B 1988 *Phil. Mag.* **58** 809–16
[10] Peryronneau J and Poirier J P 1989 *Nature* **342** 537–9
[11] Li X and Jeanloz R 1987 *Geophys. Res. Lett.* **14** 1075–8
[12] Li X and Jeanloz R 1990 *J. Geophys. Res.* **95** 5067–78
[13] Li X and Jeanloz R 1991 *J. Geophys. Res.* **96** 6113–20
[14] Matsui M and Price G D 1991 *Nature* **351** 735–7
[15] Schultz H 1982 *Ann. Rev. Mater. Sci.* **12** 351–76
[16] Gillan M J 1985 *Physica* B **131** 157–74
[17] Rahman A 1979 *Fast Ion Conductors* ed P Vashishta, J N Mundy and G K Shenoy (Amsterdam: North-Holland) pp 643–8
[18] Evangelakis G A and Pontikis V 1991 *Phys. Rev.* B **43** 3180–7
[19] Alder B J and Wainwright T W 1959 *J. Chem. Phys.* **31** 459
[20] Gear C W 1971 *Numerical Initial Value Problems in Ordinary Differential Equations* (Englewood Cliffs, NJ: Prentice-Hall)
[21] Parrinello M and Rahman A 1981 *J. Appl. Phys.* **52** 7182–90
[22] Nose S 1984 *J. Chem. Phys.* **81** 511–9
[23] Nose S 1990 *J. Phys.: Condens. Matter* **2** SA115–9
[24] Catlow C R A, Norgett M J and Ross T A 1977 *J. Phys. C: Solid State Phys.* **10** 1627–40
[25] Becher R R, Sangster M J L and Strauch D 1989 *J. Phys.: Condens. Matter* **1** 7801–17
[26] Parker S C and Price G D 1989 *Adv. Solid State Chem.* **1** 295–327
[27] O'Keeffe M 1973 *Fast Ion Transport in Solids* ed Gool (Amsterdam: North-Holland) p 244
[28] *Landolt–Bornstein New Series* 1973 Group III, vol 7 (Berlin: Springer)
[29] Insight II version 1.1.0 (Biosym. Tech. Inc.)
[30] Catlow C R A, Dixon M and Mackrodt W C 1982 *Computer Simulation of Solids* ed C R A Catlow and W C Mackrodt (Berlin: Springer) pp 130–61